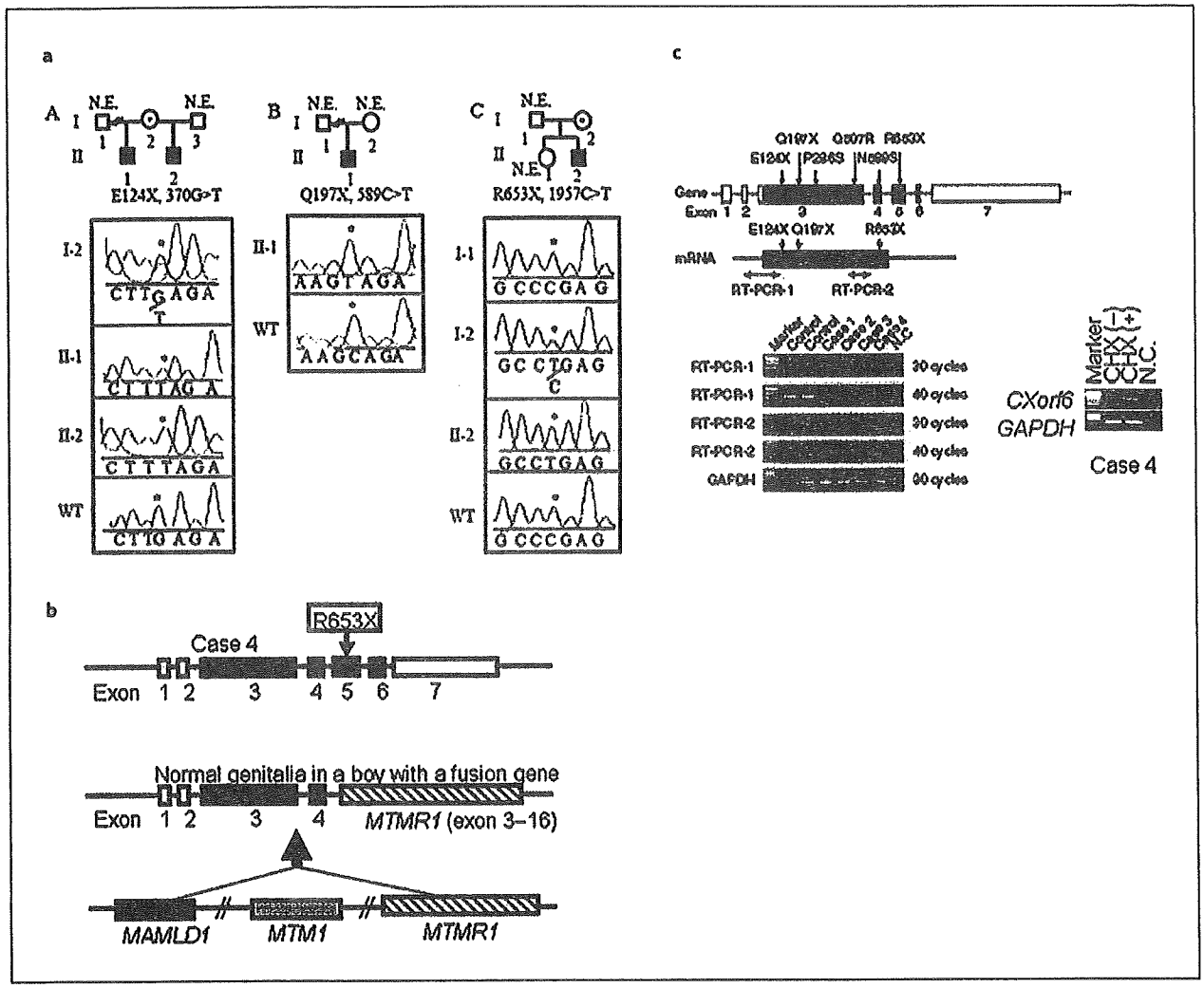

Fig. 2. Molecular findings in patients with nonsense mutations. **a**, **b** adapted from Fukami et al. [8, 9]. **a** The pedigrees and electrochromatograms of Japanese patients with nonsense mutations (A–C). The black squares indicate the patients with 46,XY DSD and the mutant *MAMLD1*, and the circles with dots represent molecularly confirmed carrier females. The asterisks in the chromatograms indicate the mutant and the corresponding wild-type nucleotides. NE = Not examined. **b** Schematic representation of the R653X mutation in case 4 and the fusion gene between *MAMLD1* and *MTMR1*. The black and the white squares in *MAMLD1* indicate the translated and untranslated regions, respectively. **c** The NMD analysis. The black and gray boxes represent the coding regions, and the open boxes denote the untranslated regions. The positions of the mutations and variations are shown. RT-PCR for the two regions (RT-PCR-1 and 2) has produced no bands after 30 cycles and very faint bands after 40 cycles in cases 1–4. In case 4, no band is seen without an NMD inhibitor cycloheximide (CHX), whereas a clear band is delineated with CHX treatment.

nally related half brothers from family A (cases 1 and 2); Q197X in a patient from family B (case 3), and R653X in a patient from family C (case 4; fig. 2a) [3]. The mothers of families A and C were heterozygous for the mutations, although the mother of family B was not studied. In addition to the 3 nonsense mutations, we also found 3 apparently non-pathologic variants: P286S and Q507R that were not co-segregated with the 46,XY DSD in affected families, and a previously reported polymorphism N589S *(rs2073043)* [3].

Table 1. Clinical findings of the 4 Japanese cases with *MAMLD1* nonsense mutations

	Case 1	Case 2	Case 3	Case 4
Genital findings				
Gestational age, weeks	39	40	40	41
Birth length, cm	51.0 (+1.0 SD)	49.5 (+0.2 SD)	50.5 (+0.7 SD)	47.5 (–0.7 SD)
Birth weight, kg	3.61 (+1.5 SD)	3.40 (+1.0 SD)	3.21 (+0.5 SD)	2.94 (–0.2 SD)
Age at exam	4 months	1 month	2 years	1 month
Clinical diagnosis	Hypospadias with chordee	Hypospadias with chordee	Hypospadias with chordee	Hypospadias with chordee
Urethral meatus	Penoscrotal junction	Penoscrotal junction	Penoscrotal junction	Penoscrotal junction
Age at urethroplasty, years	2.5	3.9	6.0 and 6.6	1.9
Penile length, cm	2.5 (–1.5 SD)	2.5 (–1.5 SD)	2.0 (–3.4 SD)	1.2 (–3.5 SD)
Testis size, ml	1–2 (B) (WNR)	1–2 (B) (WNR)	1 (B) (WNR)	1–2 (B) (WNR)
Testis position	Inguinal (B)	Scrotal	Scrotal	Retractile (B)
Age at orchidopexy, years	6.3	–	–	1.9
Scrotal appearance	Bifid and hypoplastic	Bifid	Bifid	Bifid
Wolffian structures	Normal on MRI	Normal on MRI	NE	NE
Müllerian structures	Absent on MRI	Absent on MRI	NE	NE
Renal structures	Normal on MRI	Normal on MRI	Normal on ultrasounds	NE
Serum hormone values				
Age at exam	4 months	1 month	2 years	3 months
LH, IU/l	1.2 (0.1–4.7)	3.1 (0.1–4.7)	0.2 (<0.2–3.1)	NE
FSH, IU/l	1.5 (0.4–5.7)	2.2 (0.4–5.7)	1.6 (0.2–5.2)	NE
Testosterone, nmol/l	1.4 (0.1–12.0)→9.0 (7.0–15.0)[a]	9.0 (4.0–14.0)	0.1 (0.1–1.0)	9.4 (4.0–14.0)
DHT, nmol/l	0.8 (0.2–4.5)→3.7 [a]	1.2 (0.2–4.5)	NE	NE
Age at exam, years:months	2:05	2:05	4:00	6:03
LH, IU/l	0.2 (<0.2–3.1)→3.5 (1.4–6.0)[b]	0.2 (<0.2–3.1)	<0.2 (<0.2–1.2)	0.2 (<0.2–1.4)
FSH, IU/l	<0.2 (0.2–5.2)→1.5 (2.3–6.9)[b]	0.8 (0.2–5.2)	1.6 (0.7–3.0)	1.2 (0.3–4.0)
Testosterone, nmol/l	<0.3 (0.1–1.0)→10.1 (7.0–15.0)[a]	0.7 (0.1–1.0)	<0.3 (<0.5)	0.3 (<0.5)
DHT, nmol/l	0.07 (0.05–2.0)→2.84[a]	<0.15 (0.05–2.0)	NE	NE

SD = Standard deviation; NE = not examined; B = bilateral; MRI = magnetic resonance imaging; WNR = within the normal range (1–2 ml before puberty); ND = not determined; LH = luteinizing hormone; FSH = follicle-stimulating hormone; DHT = dihydrotestosterone.

Assessments of body sizes (length, height, weight, and head circumference), penile length, testis size, and menarchial age are based on the Japanese reference data. The hormone values in parentheses represent the age- and sex-matched normal range in the Japanese; the reference data for serum hormones are based on the literature.

[a] After a human chorionic gonadotropin stimulation (3,000 IU/m^2/dose i.m. for 3 consecutive days; blood sampling on day 4).

[b] Peak values during a gonadotropin-releasing hormone test (100 μg/m^2 bolus i.v.; blood sampling at 0, 30, 60, 90, and 120 min).

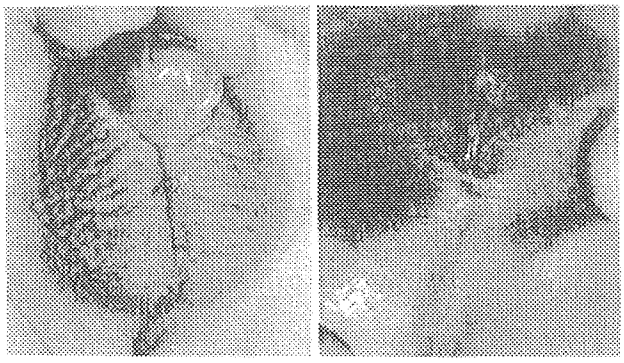

Fig. 3. External genital findings of cases 1 and 2.

Nonsense-Mediated mRNA Decay

When the 3 nonsense mutations were identified, one problem was that hypospadias in case 4 with R653X on exon 5 may be inconsistent with apparently normal genital development in a previously reported boy with a microdeletion involving *MTM1* that resulted in the generation of a fusion gene between exons 1–4 of *MAMLD1* and exons 3–16 of *MTMR1* (locus order: *MAMLD1-MTM1-MTMR1*), because the coding exons 3 and 4 are preserved in both case 4 and the boy with the fusion gene [15] (fig. 2b). However, in contrast to the positive expression of the fusion gene [15], the 3 nonsense mutations are predicted to cause nonsense-mediated mRNA decay (NMD) because of their positions [16]. Consistent with this, RT-

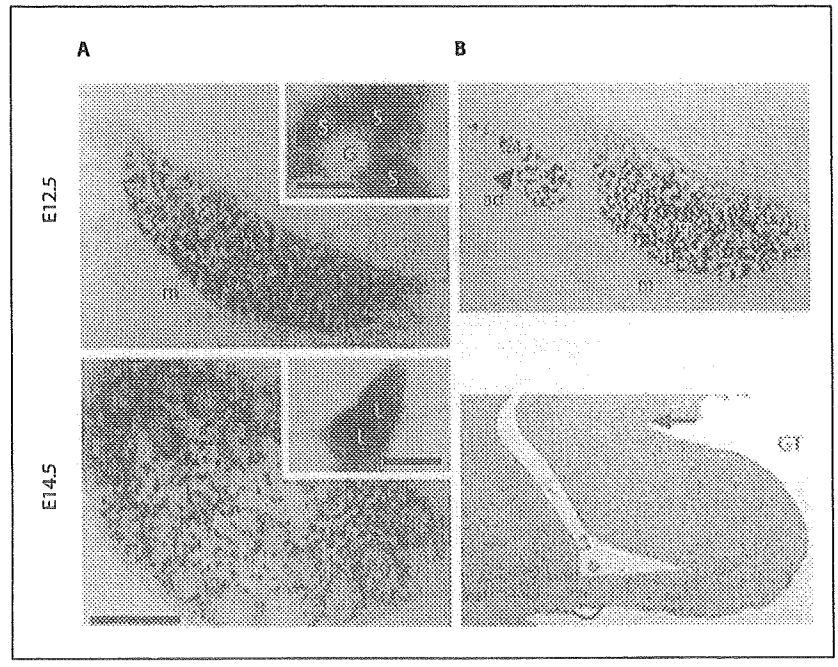

Fig. 4. In situ hybridization analysis of the murine *Mamld1*. **a** Expression patterns in the fetal testes at E12.5 and E14.5. The blue signals are derived from in situ hybridization for *Mamld1*, and the brown signals from immunohistochemical staining with Sf-1 (Ad4bp) antibodies. m = Mesonephros; G = germ cell; S = Sertoli cell; L = Leydig cell. The scale bars in the low and high power fields represent 200 and 20 μm, respectively. Adapted from Fukami et al. [8]. **b** Expression patterns in the fetal adrenal (upper part) and external genitalia (lower part) of male mouse at E12.5. m = Mesonephros; g = gonad; ad = adrenal; GT = genital tubercle (the region between two arrows). *MAMLD1* is not expressed in the adrenal, and weakly and diffusely expressed in the external genitalia as in other non-genital skin tissues.

PCR from leukocytes indicated drastically reduced transcripts in cases 1–4 (fig. 2c) [3, 4]. Furthermore, the NMD was prevented by the NMD inhibitor cycloheximide, providing further support for the occurrence of NMD in the 3 nonsense mutations. The occurrence of NMD was also demonstrated in the carrier mothers [4]. Thus, although the NMD has not been confirmed in the testicular tissue, the results explain the apparent discordance in the genital development between case 4 and the boy described by Tsai et al. [15], and indicate that the 3 nonsense mutations including R653X are pathologic mutations.

Phenotypes in Mutation-Positive Patients

Cases 1–4 had penoscrotal hypospadias with chordee as the conspicuous genital phenotype, in association with other genital phenotypes (fig. 3, table 1). Pituitary-gonadal serum hormone values remained within the normal range, including the human chorionic gonadotropin (hCG)-stimulated testosterone value in case 1 at 2 years and 5 months of age, and the basal testosterone values in case 2 at 1 month of age and in case 4 at 3 months of age when serum testosterone is physiologically elevated. Thus, the diagnosis of idiopathic hypospadias was initially made in cases 1–4.

In situ Hybridization Analysis for Mouse *Mamld1*

In situ hybridization analysis for mouse *Mamld1* showed a cell type-specific expression pattern [3]. Namely, *Mamld1* is specifically and transiently expressed in Sertoli and Leydig cells around the critical period of sex development (E12.5–E14.5; fig. 4a). This expression pattern has been confirmed by double staining with antibodies for Ad4bp/Sf-1 that serves as a marker for Sertoli and Leydig cells [17–19]. In extragonadal tissues at E12.5, *Mamld1* expression was absent in the adrenals and weakly and diffusely identified in the external genital region including the genital tubercle at a level similar to that detected in the neighboring extragenital tissues (fig. 4b). *Mamld1* was also clearly expressed in the müllerian ducts, forebrain, somite, neural tube, and pancreas. By contrast, *Mamld1* expression was absent in the postnatal testes. These data imply that nonsense mutations of *MAMLD1* cause hypospadias primarily because of transient testicular dysfunction and resultant compromised testosterone production around the critical period of sex development, and explain why postnatal endocrine data were normal in cases 1–4.

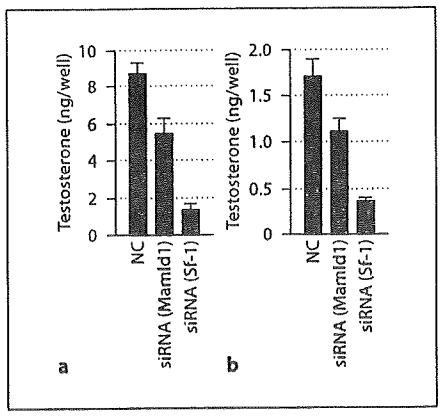

Fig. 5. Effects of siRNA on testosterone production in the mouse Leydig tumor (MLT) cells. Adapted from Fukami et al. [9]. Relative mouse *CXorf6* and *Sf-1* mRNA levels have been reduced to 25–30% in the MLT cells after 48 h of incubation with two siRNAs. NC = Negative control transfected with non-targeting RNA. **a** Testosterone concentration in the medium after 48 h of incubation with siRNAs. **b** Testosterone concentration in the medium after 1 h of incubation with hCG using the MLT cells cultured with siRNA for 48 h.

Function of *Mamld1* in Testosterone Production

We performed knockdown analysis with siRNAs for *Mamld1* using mouse Leydig tumor cells that retain the capability of testosterone production and the responsiveness to hCG stimulation [4]. When the mRNA level of endogenous *Mamld1* was severely reduced in the mouse Leydig tumor cells (25–30%), testosterone production was decreased to 50–60% after 48 h of incubation and 1 h after hCG stimulation (fig. 5). However, the testosterone reduction was much milder than that caused by siRNAs for *Sf-1* (fig. 5; our unpublished observation). The results were confirmed with 2 different siRNAs. This implies that *MAMLD1* is involved in testosterone biosynthesis. Furthermore, since testosterone production would probably be attenuated rather than abolished in the absence of *MAMLD1*, this is consistent with the hypospadias phenotype in the affected patients [2].

Sf-1 Controls *Mamld1*

Mouse *Mamld1* is co-expressed with *Ad4bp/Sf-1*, and *SF-1* is known to regulate the transcription of a vast array of genes involved in sex development by binding to specific DNA sequences [17–19]. This implies that *Mamld1* is also controlled by *Sf-1*. Consistent with this notion, human *MAMLD1* harbors a putative SF-1-binding sequence 'CCAAGGTCA' at intron 2 upstream of the coding region [4]. This binding site also resides at intron 1 upstream of the coding region of the mouse *Mamld1*. Furthermore, we performed DNA binding and luciferase assays, showing that SF-1 protein binds to the putative target sequence and exerts a transactivation function [4]. These findings argue for the possibility that Mamld1 expression is regulated by *Sf-1*.

Functional Studies of MAMLD1 Protein

We found that MAMLD1 protein has a unique structure with homology to that of mastermind like 2 (MAML2) protein (fig. 6a) [4]. A unique amino acid sequence, which we designate mastermind-like (MAML) motif, was inferred from sequence alignment with MAML1, MAML2, and MAML3 proteins. The MAML motif was well conserved among MAMLD1 orthologs identified in frogs, birds, and mammals. In addition, glutamine-rich, proline-rich, and serine-rich domains were identified in MAMLD1.

MAML2 is a non-DNA-binding transcriptional coactivator in Notch signaling that plays an important role in cell differentiation in multiple tissues by exerting either inductive or inhibiting effects according to the context of the cells [20–22]. Upon ligand-receptor interaction, the Notch intracellular domain (N-ICD) is translocated from the cell surface to the nucleus and interacts with a DNA-binding transcription factor, recombination signal binding protein-J (RBP-J), to activate target genes like hairy/enhancer of split 1 *(Hes1)* and *Hes5* [23]. In this canonical Notch signaling process, MAML2 forms a ternary complex with N-ICD and RBP-J at nuclear bodies, enhancing the transcription of the Notch target genes [20, 21, 24–26]. In addition to such canonical Notch target genes, recent studies have shown that *Hes3* can be induced by stimulation with a Notch ligand, via a STAT3 (signal transducer and activator of transcription 3)-mediated pathway [27]. This finding, together with lack of *Hes3* induction by N-ICD [22], implies that *Hes3* represents a target gene of a non-canonical Notch signaling.

Thus, we first examined whether MAMLD1 localizes to the nuclear bodies, as observed for MAML2 [4]. Since PCR-based human cDNA library screening has revealed that the exon 4-positive splice variant is more strongly expressed than the exon 4-negative splice variant (ΔExon 4) [3], functional studies were performed primarily with

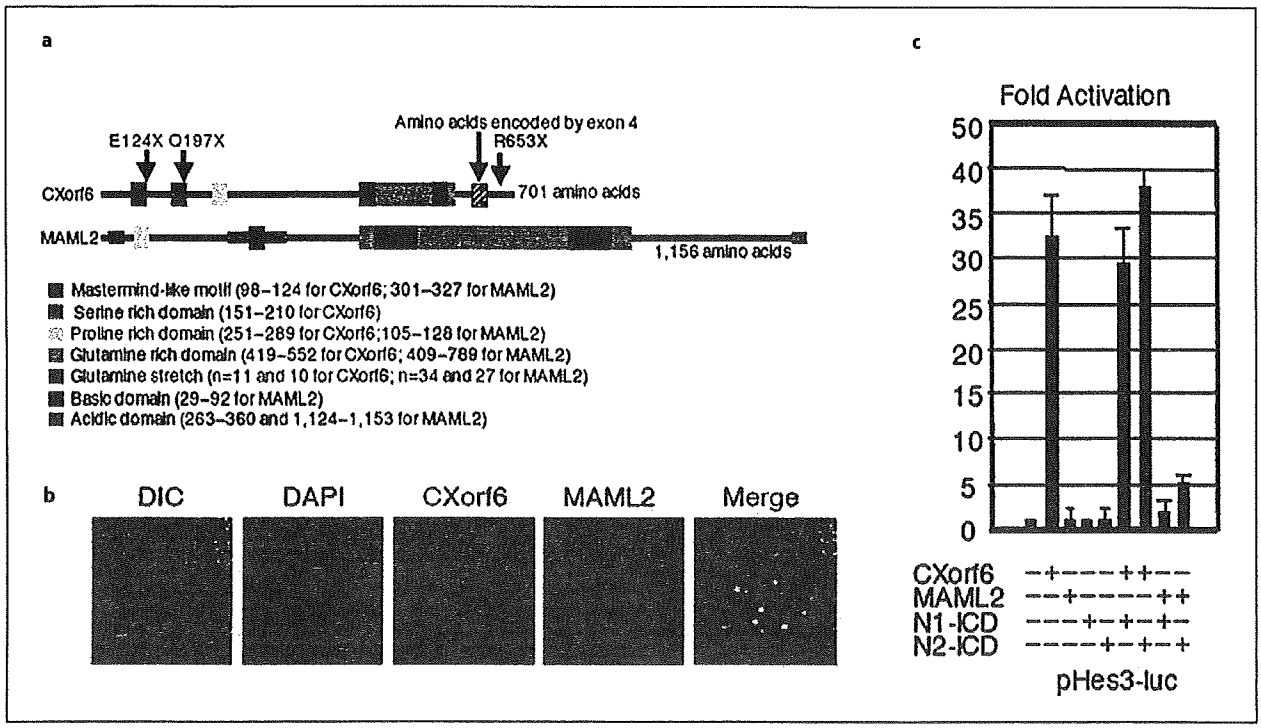

Fig. 6. Functional studies of the wild-type MAMLD1 protein. Adapted from Fukami et al. [9]. **a** Protein structure analysis. The structure of human CXorf6 (MAMLD1) and MAML2 proteins. The identified domains are shown, together with the positions of the three nonsense mutations. **b** Subcellular localization analysis, showing co-localization of the wild-type MAMLD1 and MAML2 in the nuclear bodies. **c** Transactivation functions for the promoter of *Hes3*. + = Presence of expression vectors with cDNAs for *MAMLD1, MAML2, N1-ICD* (Notch 1 intracellular domain), and *N2-ICD* (Notch 2 intracellular domain); − = presence of expression vector only (empty).

the exon 4-positive splice variant (thereafter, this variant is simply described as *MAMLD1*). MAMLD1 was distributed in a speckled pattern and co-localized with the MAML2 protein (fig. 6b). Furthermore, while the E124X and Q197X fusion proteins resided in the nucleus, they were incapable of localizing to the nuclear bodies. The R653X and apparently non-pathologic missense proteins showed a punctate pattern, and co-localized with the wild-type MAMLD1.

Next, we studied whether MAMLD1 has a transactivation function for Notch targets using luciferase reporter assays [4]. Although MAMLD1 was incapable of enhancing the promoter activities of the canonical Notch target genes *Hes1* and *Hes5* with the RBP-J-binding site [22], MAMLD1 transactivated the promoter activity of the non-canonical Notch target gene *Hes3* without the RBP-J-binding site (fig. 6c) [28]. These results argue that MAMLD1 exerts its transactivation activity independent of RBP-J-binding sites. Thus, while it was predicted that MAMLD1 protein has a DNA-binding capacity, after extensive analysis, no evidence has been obtained for a positive DNA binding of MAMLD1 [4].

Furthermore, the E124X and Q197X proteins had no transactivation function, whereas the R653X protein as well as the 3 variant (P286S, Q507R, and N589S) proteins retained a nearly normal transactivating activity [4]. In addition, the transactivation function was significantly reduced in the L103P protein (an artificially constructed variant affecting the MAML motif) and normal in the ΔExon 4 [4]. These findings suggest that the E124X and Q197X proteins have no transactivation function, consistent with the inability of localizing to the nuclear bodies. However, the R653X protein, when it is artificially produced, has a normal transactivating activity, although R653X as well as E124X and Q197X have been demonstrated to undergo NMD in vivo [3, 4].

Conclusions

MAMLD1 is a causative gene for hypospadias, and possibly other forms of 46,XY DSD. It appears to play a supportive role in the testosterone production around the critical period of sex development. MAMLD1 protein localizes to the nuclear bodies and has a transactivation function for *Hes3* at least in vitro. Further studies including knockout mouse experiments will enable clarification of the *MAMLD1*-dependent molecular network involved in testosterone production.

References

1 Baskin LS, Ebbers MB: Hypospadias: anatomy, etiology, and technique. J Pediatr Surg 2007;41:463–472.
2 Achermann JC, Hughes IA: Disorders of sex development; in Kronenberg HM, Melmed S, Polonsk KS, Larsen PR (eds): Williams Textbook of Endocrinology, ed 11. Philadelphia, Saunders, 2008, pp 783–848.
3 Beleza-Meireles A, Töhönen V, Söderhäll C, Schwentner C, Radmayr C, Kockum I, Nordenskjöld A: Activating transcription factor 3: a hormone responsive gene in the etiology of hypospadias. Eur J Endocrinol 2008;158:729–739.
4 Beleza-Meireles A, Barbaro M, Wedell A, Töhönen V, Nordenskjöld A: Studies of a cochaperone of the androgen receptor, FKBP52, as candidate for hypospadias. Reprod Biol Endocrinol 2007;5:8.
5 Beleza-Meireles A, Lundberg F, Lagerstedt K, Zhou X, Omrani D, Frisén L, Nordenskjöld A: FGFR2, FGF8, FGF10 and as candidate genes for hypospadias. Eur J Hum Genet 2007;15:405–410.
6 Watanabe M, Yoshida R, Ueoka K, Aoki K, Sasagawa I, Hasegawa T, Sueoka K, Kamatani N, Yoshimura Y, Ogata T: Haplotype analysis of the estrogen receptor 1 gene in male genital and reproductive abnormalities. Hum Reprod 2007;22:1279–1284.
7 Beleza-Meireles A, Kockum I, Lundberg F, Söderhäll C, Nordenskjöld A: Risk factors for hypospadias in the estrogen receptor 2 gene. J Clin Endocrinol Metab 2007;92:3712–3718.
8 Fukami M, Wada Y, Miyabayashi K, Nishino I, Hasegawa T, Nordenskjöld A, Camerino G, Kretz C, Buj-Bello A, Laporte J, Yamada G, Morohashi K, Ogata T: CXorf6 is a causative gene for hypospadias. Nat Genet 2006;38:1369–1371.
9 Fukami M, Wada Y, Okada M, Kato F, Katsumata N, Baba T, Morohashi K, Laporte J, Kitagawa M, Ogata T: Mastermind-like domain-containing 1 (MAMLD1 or CXorf6) transactivates the Hes3 promoter, augments testosterone production, and contains the SF1 target sequence. J Biol Chem 2008;283:5525–5532.
10 Bartsch O, Kress W, Wagner A, Seemanova E: The novel contiguous gene syndrome of myotubular myopathy (MTM1), male hypogenitalism and deletion in Xq28: report of the first familial case. Cytogenet Cell Genet 1999;85:310–314.
11 Biancalana V, Caron O, Gallati S, Baas F, Kress W, Novelli G, D'Apice MR, Lagier-Tourenne C, Buj-Bello A, Romero NB, Mandel JL: Characterisation of mutations in 77 patients with X-linked myotubular myopathy, including a family with a very mild phenotype. Hum Genet 2003;112:135–142.
12 Hu LJ, Laporte J, Kress W, Kioschis P, Siebenhaar R, Poustka A, Fardeau M, Metzenberg A, Janssen EA, Thomas N, Mandel JL, Dahl N: Deletions in Xq28 in two boys with myotubular myopathy and abnormal genital development define a new contiguous gene syndrome in a 430 kb region. Hum Mol Genet 1996;5:139–143.
13 Laporte J, Guiraud-Chaumeil C, Vincent MC, Mandel JL, Tanner SM, Liechti-Gallati S, Wallgren-Pettersson C, Dahl N, Kress W, Bolhuis PA, Fardeau M, Samson F, Bertini E: Mutations in the MTM1 gene implicated in X-linked myotubular myopathy. Hum Mol Genet 1997;6:1505–1511.
14 Laporte J, Kioschis P, Hu LJ, Kretz C, Carlsson B, Poustka A, Mandel JL, Dahl N: Cloning and characterization of an alternatively spliced gene in proximal Xq28 deleted in two patients with intersexual genitalia and myotubular myopathy. Genomics 1997;41:458–462.
15 Tsai TC, Horinouchi H, Noguchi S, Minami N, Murayama K, Hayashi YK, Nonaka I, Ishino I: Characterization of MTM1 mutations in 31 Japanese families with myotubular myopathy, including a patient carrying 240 kb deletion in Xq28 without male hypogenitalism. Neuromuscul Disord 2005;15:245–252.
16 Kuzmiak HA, Maquat LE: Applying nonsense-mediated mRNA decay research to the clinic: progress and challenges. Trends Mol Med 2006;12:306–316.
17 Morohashi K, Omura T: Ad4BP/SF-1, a transcription factor essential for the transcription of steroidogenic cytochrome P450 genes and for the establishment of the reproductive function. FASEB J 1996;10:1569–1577.
18 Ozisik G, Achermann JC, Jameson JL: The role of SF1 in adrenal and reproductive function: insight from naturally occurring mutations in humans. Mol Genet Metab 2002;76:85–91.
19 Parker KL, Schimmer BP: Steroidogenic factor 1: a key determinant of endocrine development and function. Endocr Rev 1997;18:361–377.
20 Lin SE, Oyama T, Nagase T, Harigaya K, Kitagawa M: Identification of new human mastermind proteins defines a family that consists of positive regulators for notch signaling. J Biol Chem 2002;277:50612–50620.
21 Wu L, Sun T, Kobayashi K, Gao P, Griffin JD: Identification of a family of mastermind-like transcriptional coactivators for mammalian notch receptors. Mol Cell Biol 2002;22:7688–7700.
22 Artavanis-Tsakonas S, Rand MD, Lake RJ: Notch signaling: cell fate control and signal integration in development. Science 1999;284:770–776.
23 Iso T, Kedes L, Hamamori Y: HES and HERP families: multiple effectors of the Notch signaling pathway. J Cell Physiol 2003;194:237–255.
24 Nam Y, Sliz P, Song L, Aster JC, Blacklow SC: Structural basis for cooperativity in recruitment of MAML coactivators to Notch transcription complexes. Cell 2006;124:973–983.
25 Wilson JJ, Kovall RA: Crystal structure of the CSL-Notch-Mastermind ternary complex bound to DNA. Cell 2006;124:985–996.
26 Tonon G, Modi S, Wu L, Kubo A, Coxon AB, Komiya T, O'Neil K, Stover K, El-Naggar A, Griffin JD, Kirsch IR, Kaye FJ: t(11; 19)(q21; p13) translocation in mucoepidermoid carcinoma creates a novel fusion product that disrupts a Notch signaling pathway. Nat Genet 2003;33:208–213.
27 Androutsellis-Theotokis A, Leker RR, Soldner F, Hoeppner DJ, Ravin R, Poser SW, Rueger MA, Bae SK, Kittappa R, McKay RD: Notch signalling regulates stem cell numbers in vitro and in vivo. Nature 2006;442:823–826.
28 Nishimura M, Isaka F, Ishibashi M, Tomita K, Tsuda H, Nakanishi S, Kageyama R: Structure, chromosomal locus, and promoter of mouse Hes2 gene, a homologue of Drosophila hairy and Enhancer of split. Genomics 1998;49:69–75.

Endocrine Journal 2010, 57 (2), 171-174

Diabetes Mellitus in a Japanese Girl with HDR Syndrome and *GATA3* Mutation

KOJI MUROYA[1), 2)], TAKAHIRO MOCHIZUKI[3)], MAKI FUKAMI[1)], MANAMI ISO[1)], KEINOSUKE FUJITA[3)], MITSUO ITAKURA[4)] AND TSUTOMU OGATA[1)]

[1)] *Department of Endocrinology and Metabolism, National Research Institute for Child Health and Development, Tokyo, Japan*
[2)] *Department of Endocrinology and Metabolism, Kanagawa Children's Medical Center, Yokohama, Japan*
[3)] *Department of Pediatrics, Children's Medical Center, Osaka City General Hospital, Osaka, Japan*
[4)] *Institute for Genome Research, Tokushima University, Tokushima, Japan*

Abstract. We report on a Japanese girl with HDR (*h*ypoparathyroidism, sensorineural *d*eafness, and *r*enal dysplasia) syndrome who developed diabetes mellitus (DM) at three years of age (blood glucose 713 mg/dL, HbA_{1c} 8.0%) in the absence of anti-glutamic acid decarboxylase autoantibodies. Mutation analysis revealed a *de novo* heterozygous two base pair deletion at exon 6 of the *GATA3* gene (c.1200_1201delCA; p.H400fsX506). *GATA3* expression was identified by PCR amplification for human pancreas cDNA, and mouse *Gata3* was weekly but unequivocally expressed in pancreatic β cells. The results, in conjunction with the previous findings indicating the critical role of *GATA3* in lymphocyte function, suggest that *GATA3* haploinsufficiency may affect the function of β cells and/or lymphocytes, leading to the development of DM in relatively exceptional patients with high susceptibility to DM.

Key words: Diabetes mellitus, Expression, *GATA3*, HDR syndrome

HDR (*h*ypoparathyroidism, sensorineural *d*eafness, and *r*enal dysplasia) syndrome is an autosomal dominant disorder first reported by Bilous *et al.* [1]. This condition is primarily caused by haploinsufficiency of *GATA3* on chromosome 10p15, although a *GATA3* mutation has not been identified in several patients with HDR syndrome-compatible clinical features [2, 3]. *GATA3* consists of six exons, and encodes a transcription factor with two transactivation domains and two zinc finger domains [2]. *GATA3* is expressed in the developing parathyroid glands, inner ears, and kidneys, together with thymus and central nervous system [4, 5]. While several non-triad features such as pyloric stenosis, ventricular septal defect, polycystic ovary, abnormal Müllerian duct structures, and hemimegalencephaly have been described in several patients with *GATA3* mutations [3, 6–8], there is no report documenting diabetes mellitus (DM) in this condition.

Here, we report a patient with DM and a *GATA3* mutation, and discuss a potential relationship between DM and a *GATA3* mutation.

Received Oct. 26, 2009; Accepted Nov. 19, 2009 as K09E-313
Released online in J-STAGE as advance publication Dec. 1, 2009

Correspondence to: Dr. Tsutomu OGATA, Department of Endocrinology and Metabolism, National Research Institute for Child Health and Development, 2-10-1 Ohkura, Setagaya, Tokyo 157-8535, Japan. E-mail: tomogata@nch.go.jp

Case Report

This Japanese girl was born at 37 weeks of gestation after an uncomplicated pregnancy and delivery. At birth, her length was 43.0 cm (–2.4 SD) and her weight 1.74 kg (–3.1 SD). The non-consanguineous parents and the younger brother were clinically normal.

At 3 months of age, she was admitted to Osaka City Medical Center because of frequent vomiting and irritability. Routine laboratory tests revealed hypocalcemia (7.8 mg/dL) (age- and sex-matched Japanese reference value, 9.8–11.6 mg/dL) and hyperphosphatemia (8.3 mg/dL) (5.1–7.1 mg/dL), and subsequent biochemical studies showed parathyroid hormone (PTH) deficiency (intact PTH, below 5 pg/mL) (10–50 pg/mL). Thus, 1α-(OH) vitamin D therapy was started, successfully normalizing serum calcium and phosphate values. At 12 months of age, since she

responded poorly to sounds, auditory brainstem response was performed, indicating severe sensorineural deafness with hearing levels being 80 dB for the right ear and 100 dB for the left ear (normal range, below 25 dB). Thus, hearing aids were utilized in her daily life.

At 3 years of age, she showed polydipsia, polyuria, and weight loss, and was diagnosed as having DM because of elevated blood glucose (713 mg/dL) (70–110 mg/dL) and HbA_{1c} (8.0%) (4.3–5.8%). Serum insulin was 8.0 μU/mL (1.7–10.4μU/mL) and C-peptide 1.1 ng/mL (0.6–1.8 ng/mL). She was immediately placed on insulin therapy (~0.7 U/kg/day). Urine C-peptide gradually decreased and became undetectable at eight years of age; at that time, she required insulin therapy of 1.08 U/kg/day. Anti-glutamic acid decarboxylase autoantibodies (anti-GAD Abs) were negative throughout the clinical course. At nine years of age, she was found to have elevated blood urea nitrogen (61.3 mg/dL) (7.5–19.3 mg/dL) and creatinine (2.0 mg/dL) (0.4–0.8 mg/dL) at the time of periodical follow-up examinations for DM. Thus, renal echography and scntigraphy were performed, showing right renal aplasia and left renal hypoplasia. Other abdominal visceral organs including the pancreas exhibited apparently normal structures on the ultrasound examinations. Chromosome analysis revealed a 46,XX karyotype in all the 50 lymphocytes examined. On the basis of the above findings, she was diagnosed as having HDR syndrome and DM. At present, she is 12 years old, and shows short stature (–4.5 SD) and some pubertal development (breast, Tanner stage 2). Current insulin dosage is 1.17 U/kg/day, and her DM has been well controlled with HbA1c value being maintained around 6.0%.

Methods

Mutation analysis of GATA3

This study was approved by the Institutional Review Board Committee at National Center for Child Health and Development. After obtaining informed consent, leukocyte genomic DNA samples of the patient and the parents were PCR-amplified for the coding exons 2–6 and their splice sites, and the PCR products were subjected to direct sequencing from both directions on a CEQ 8000 autosequencer (Beckman Coulter, Fullerton, CA). The primer sequences and the PCR conditions were as described previously [2, 3]. To confirm a heterozygous mutation, the corresponding PCR products were subcloned with a TOPO TA Cloning Kit (Invitrogen, Carlsbad, CA), and normal and mutant alleles were sequenced separately.

PCR amplification of human pancreas cDNA

Human pancreas cDNA was purchased from Clontech (Mountain View, CA), as well as fetal kidney cDNA utilized as a positive control. PCR amplification was performed with 0.5 ng of cDNA samples, using the forward primer for exon 5 (5'–GAATGCCA-ATGGGGACCCTGT–3') and the reverse primer for exon 6 (5'–TTCATGCCTTACAGCTACCCAGA–3').

In situ hybridization (ISH) analysis for the mouse pancreas

Fifteen-week-old female BDF1 mice (Clea Japan, Tokyo) were anesthetized with sodium pentobarbital and fixed by cardiac perfusion with Mildform10N (Wako Pure Chemical Industries, Osaka). Pancreatic tissues were dissected and fixed with the same fixative for 48 hours at room temperature. The tissues were embedded in paraffin, and serial tissue sections were prepared at 5 μm thickness. ISH analysis was performed with BlueMap Kit and Discovery automatic staining modules (Ventana Medical Systems, Tucson, AZ) according to manufacturer's instructions. cDNAs of mouse *Ins-1* (an insulin-like peptide orthologous to human insulin) (nt 653–1117, GenBank accession no. X04725) and *Gata3* (nt 1566–2002, GenBank accession no. NM_008091) were amplified by reverse transcription PCR and subcloned into pCR4Blunt-TOPO (Invitrogen). Sense and antisense digoxigenin-labeled RNA probes were synthesized using T7 or T3 RNA polymerase in the presence of digoxigenin-labeled dUTP following the manufacturer's protocol (Roche Molecular Biochemicals, Indianapolis, IN).

Results

Mutation analysis of GATA3

This patient had a heterozygous two base pair deletion at exon 6 (c.1200_1201delCA) of *GATA3* that is predicted to cause a frameshift at the 400th codon for the histidine and resultant termination at the 506th codon (p.H400fsX506) (Fig. 1). This mutation was absent from the parents.

PCR amplification of human pancreas cDNA

PCR products of 690 bp long were identified in fe-

tal kidney after 25 cycles and in pancreas after 40 cycles (Fig. 2A). This indicated relatively weak *GATA3* expression in the pancreas.

ISH analysis for the mouse pancreas

Anti-sense probes for *Gata3* detected weak but definitive signals in cells with strong *Ins-1* expression (Fig. 2B). This showed specific *Gata3* expression in the mouse pancreatic β cells.

Discussion

This patient had the triad of the HDR syndrome and a heterozygous mutation of *GATA3*. This is consistent with the previous data indicating that *GATA3* mutations are usually identified in patients with two or three of the HDR triad features [9, 10].

The salient feature of this patient is the development of DM. This may be co-incidental, because DM has not been identified in patients with *GATA3* mutations. However, human *GATA3* was identified in the human pancreas cDNA sample, and mouse *Gata3* was weekly but unequivocally expressed in pancreatic β cells. In addition, *GATA3* is known to play an important role in lymphocyte development and function [11, 12]. Thus, *GATA3* haploinsufficiency may affect the function of β cells and/or lymphocytes, leading to the development of DM in relatively exceptional patients with high susceptibility to DM because of other genetic and environmental factors. In this regard, the absence of anti-GAD Abs may argue for possible β cell, rather than lymphocyte, dysfunction [13].

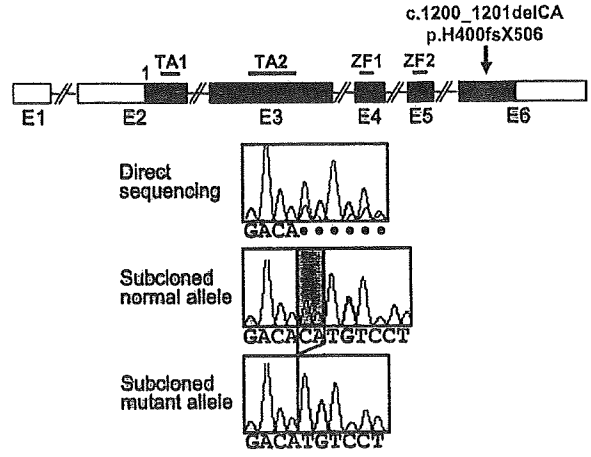

Fig. 1. Mutation analysis of *GATA3*.
Upper diagram: The genomic structure of *GATA3*. The black and white boxes denote the coding and the untranslated regions, respectively. TA1 and TA2 denote two transactivation domains, and ZF1 and ZF2 represent two zinc finger domains.
Lower diagram: The electrochromatograms delineate the c.1200_1201delCA (p.H400fsX506) mutation at exon 6. This mutation has been indicated by the direct sequencing, and confirmed by the subsequently performed sequencing of the subcloned normal and mutant alleles.

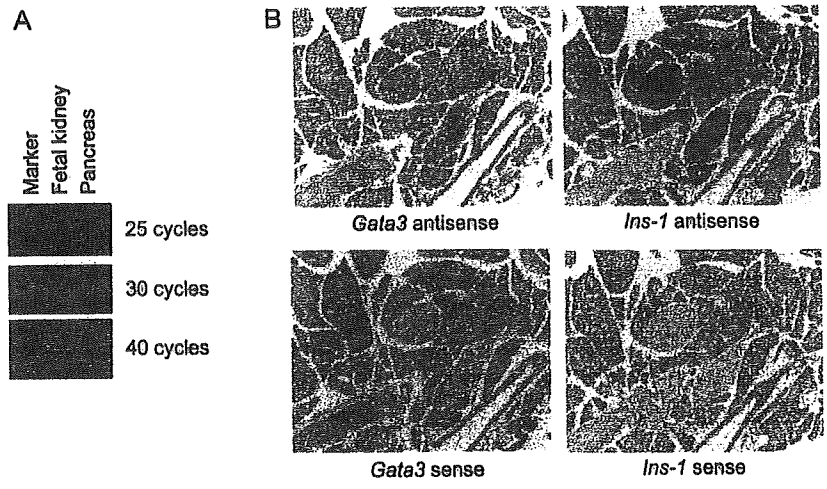

Fig. 2. Expression analyses of *GATA3/Gata3*.
A. PCR-amplification using human cDNA samples. *GATA3* expression is identified after 25 cycles in the fetal kidney, and after 40 cycles in the pancreas.
B. ISH analysis using the mouse pancreas. The antisense probe for *Gata3* detects weak but positive signals in the cells with strong expression of *Ins-1* (β cells). No signals have been identified by the sense probes.

The frameshift mutation resided on the last coding exon 6. Since the position of the mutation satisfies the condition for the escape from nonsense mediated mRNA decay [14], it is possible that an aberrant GATA3 protein is produced, leading to the development of DM due to a dominant negative effect. However, this possibility is unlikely, because previously reported patients with nonsense or frameshift mutations on exon 6 are free from DM [3, 10].

In summary, we observed a patient with a *GATA3* mutation and DM. Further studies will clarify whether *GATA3* mutations can be a risk factor for the development of DM.

Acknowledgements

This work was supported in part by grants for Child Health and Development and for Research on Children and Families from the Ministry of Health, Labor, and Welfare.

References

1. Bilous RW, Murty G, Parkinson DB, Thakker RV, Coulthard MG, Burn J, Mathias D, Kendall-Taylor P (1992) Autosomal dominant familial hypoparathyroidism, sensorineural deafness, and renal dysplasia. *N Engl J Med* 327: 1069–1074.
2. Van Esch H, Groenen P, Nesbit MA, Schuffenhauer S, Lichtner P, Vanderlinden G, Harding B, Beetz R, Bilous RW, Holdaway I, Shaw NJ, Fryns JP, Van de Ven W, Thakker RV, Devriendt K (2000) GATA3 haplo-insufficiency causes human HDR syndrome. *Nature* 406: 419–422.
3. Muroya K, Hasegawa T, Ito Y, Nagai T, Isotani H, Iwata Y, Yamamoto K, Fujimoto S, Seishu S, Fukushima Y, Hasegawa Y, Ogata T (2001) GATA3 abnormalities and the phenotypic spectrum of HDR syndrome. *J Med Genet* 38: 374–380.
4. Labastie MC, Catala M, Gregoire JM, Peault B (1995) The GATA3 gene is expressed during human kidney embryogenesis. *Kidney Int* 47: 1597–1603.
5. Debacker C, Catala M, Labastie MC (1999) Embryonic expression of the human GATA3 gene. *Mech Dev* 85: 183–187.
6. Zahirieh A, Nesbit MA, Ali A, Wang K, He N, Stangou M, Bamichas G, Sombolos K, Thakker RV, Pei Y (2005) Functional analysis of a novel GATA3 mutation in a family with the hypoparathyroidism, deafness, and renal dysplasia syndrome. *J Clin Endocrinol Metab* 90: 2445–2450.
7. Hernández AM, Villamar M, Roselló L, Moreno-Pelayo MA, Moreno F, Del Castillo I (2007) Novel mutation in the gene encoding the GATA3 transcription factor in a Spanish familial case of hypoparathyroidism, deafness, and renal dysplasia (HDR) syndrome with female genital tract malformations. *Am J Med Genet A* 143: 757–762.
8. Adachi M, Tachibana K, Asakura Y, Tsuchiya T (2006) A novel mutation in the GATA3 gene in a family with HDR syndrome (hypoparathyroidism, sensorineural deafness and renal anomaly syndrome). *J Pediatr Endocrinol Metab* 19: 87–92.
9. Nesbit MA, Bowl MR, Harding B, Ali A, Ayala A, Crowe C, Dobbie A, Hampson G, Holdaway I, Levine MA, McWilliams R, Rigden S, Sampson J, Williams AJ, Thakker RV (2004) Characterization of GATA3 mutations in the hypoparathyroidism, deafness, and renal dysplasia (HDR) syndrome. *J Biol Chem* 279: 22624–22634.
10. Ali A, Christie PT, Grigorieva IV, Harding B, Van Esch H, Ahmed SF, Bitner-Glindzicz M, Blind E, Bloch C, Christin P, Clayton P, Gecz J, Gilbert-Dussardier B, Guillen-Navarro E, Hackett A, Halac I, Hendy GN, Lalloo F, Mache CJ, Mughal Z, Ong AC, Rinat C, Shaw N, Smithson SF, Tolmie J, Weill J, Nesbit MA, Thakker RV (2007) Functional characterization of GATA3 mutations causing the hypoparathyroidism-deafness-renal (HDR) dysplasia syndrome: insight into mechanisms of DNA binding by the GATA3 transcription factor. *Hum Mol Genet* 16: 265–275.
11. Labastie MC, Bories D, Chabret C, Grégoire JM, Chrétien S, Roméo PH (1994) Structure and expression of the human GATA3 gene. *Genomics* 21: 1–6.
12. Hendriks RW, Nawijn MC, Engel JD, van Doorninck H, Grosveld F, Karis A (1999) Expression of the transcription factor GATA-3 is required for the development of the earliest T cell progenitors and correlates with stages of cellular proliferation in the thymus. *Eur J Immunol* 29: 1912–1918.
13. Eisenabrth GS, Polonsky KS, Buse JB (2008) Type 1 diabetes mellitus. In: Kronenberg HM, Melmed S, Polonsky KS, Larsen PR (eds). Williams textbook of endocrinology, 11th ed. W.B. Saunders, Philadelphia, pp 1391–1416.
14. Kuzmiak HA, Maquat LE (2006) Applying nonsense-mediated mRNA decay research to the clinic: progress and challenges. *Trends Mol Med* 12: 306–316.

Novel Insights from Clinical Practice

HORMONE RESEARCH

Horm Res 313
DOI: 10.1159/000XXXXXX

Received: September 7, 2009
Accepted: November 11, 2009
Published online: ■■■

Hypothalamic Dysfunction in a Female with Isolated Hypogonadotropic Hypogonadism and Compound Heterozygous *TACR3* Mutations and Clinical Manifestation in Her Heterozygous Mother

Maki Fukami[a] Tetsuo Maruyama[b] Sumito Dateki[a] Naoko Sato[a]
Yasunori Yoshimura[b] Tsutomu Ogata[a]

[a]Department of Endocrinology and Metabolism, National Research Institute for Child Health and Development, and
[b]Department of Obstetrics and Gynecology, Keio University School of Medicine, Tokyo, Japan

Established Facts

- *TAC3* and *TACR3* have recently been shown to be causative genes for an autosomal recessive form of isolated hypogonadotropic hypogonadism (IHH).

Novel Insights

- Hypothalamic dysfunction may be the primary cause for IHH in patients with biallelic *TACR3* mutations.
- Clinical phenotype may be exhibited by females with heterozygous *TACR3* mutations.
- *TAC3* and *TACR3* mutations remain rare in patients with IHH.

Key Words
Heterozygous manifestation · Hypogonadotropic hypogonadism · Hypothalamus · *TACR3* mutation

Abstract
Background/Aims: *TAC3* and *TACR3* have recently been shown to be causative genes for an autosomal recessive form of isolated hypogonadotropic hypogonadism (IHH). Here, we report a Japanese female with IHH and compound heterozygous *TACR3* mutations and her heterozygous parents, and discuss the primary lesion for IHH and clinical findings. ***Case Report:*** This female was identified through mutation analysis of *TAC3* and *TACR3* in 57 patients with IHH. At 24 years of age, an initial standard GnRH test showed poor gonadotropin response (LH <0.2–0.6 IU/l), whereas the second GnRH test performed after GnRH priming (100 μg i.m. for 5

This work was supported by grants from the Ministry of Health, Labor, and Welfare, and the Ministry of Education, Culture, Sports, Science, and Technology.

KARGER
Fax +41 61 306 12 34
E-Mail karger@karger.ch
www.karger.com

0301–0163/10/0000–0000$26.00/0

Accessible online at:
www.karger.com/hre

Tsutomu Ogata
Department of Endocrinology and Metabolism
National Research Institute for Child Health and Development
2-10-1 Ohkura, Setagaya, Tokyo 157-8535 (Japan)
Tel. +81 3 5494 7025, Fax +81 3 5494 7026, E-Mail tomogata@nch.go.jp

consecutive days) revealed ameliorated gonadotropin responses (LH 0.3–6.4 IU/l, FSH 2.2–9.6 IU/l). The mother exhibited several features suggestive of mild IHH, whereas the father showed an apparently normal phenotype. ***Results:*** She had a paternally derived nonsense mutation at exon 1 (Y145X) and a maternally inherited single nucleotide (G) deletion from the conserved 'GT' splice donor site of intron 1 (IVS1+1delG). ***Conclusions:*** The results suggest hypothalamic dysfunction as the primary cause for IHH in patients with biallelic *TACR3* mutations and clinical manifestation in heterozygous females, together with the rarity of *TAC3* and *TACR3* mutations in patients with IHH.

Introduction

Isolated hypogonadotropic hypogonadism (IHH) is a genetically heterogeneous condition that lacks other pituitary hormone deficiency [1]. Recently, Topaloglu et al. [2] and Guran et al. [3] have reported homozygous *TAC3* or *TACR3* missense mutations in 11 patients with IHH from 5 Turkish or Kurdish families. TAC3 belongs to an evolutionally conserved neuropeptide family, and TACR3 belongs to a G-protein-coupled receptor family [4]. Topaloglu et al. [2] and Guran et al. [3] also performed functional studies using an intracellular calcium flux system, successfully revealing markedly attenuated activities of the TAC3 and TACR3 mutant proteins. These data provide the first evidence of genetic defects in TAC3/TACR3 signaling being involved in an autosomal recessive form of IHH.

However, there is no other report of *TAC3* or *TACR3* mutations, and further studies are necessary to define the underlying factor(s) for IHH and clinical findings in *TAC3* or *TACR3* mutations. Here, we report a female with IHH and *TACR3* mutations, and discuss the primary cause for IHH and the clinical phenotypes of the patient and her heterozygous parents.

Methods

Mutation Analysis

This study was approved by the Institutional Review Board Committees at the National Center for Child Health and Development and Keio University School of Medicine. After obtaining written informed consent, leukocyte genomic DNA samples from 57 Japanese cases with IHH (38 with 46,XY and 19 with 46,XX) were PCR-amplified with the previously reported primers [2], and subjected to direct sequencing on a CEQ 8000 autosequencer (Beckman Coulter, Fullerton, Calif., USA). To confirm a heterozygous mutation, the corresponding PCR products were subcloned with a TOPO TA Cloning Kit (Invitrogen, Carlsbad, Calif., USA), and the two alleles were sequenced separately.

Prediction of Aberrant Splicing and Nonsense-Mediated mRNA Decay

We utilized the splice site prediction program at the Berkeley Drosophila Genome Project (http://www.fruitfly.org/seq_tools/splice.html) to predict aberrant splicing. On the basis of the previous report [5], we also analyzed whether identified mutations could be subject to nonsense-mediated mRNA decay (NMD) that functions as an mRNA surveillance mechanism to prevent the formation of aberrant proteins.

PCR-Based cDNA Screening for TACR3

Human cDNA samples from control subjects were prepared by RT-PCR or purchased from Clontech (Palo Alto, Calif., USA). PCR amplification was performed for *TACR3* with primers for exon 1 (5′-TTGTGAACCTGGCTTTCTCC-3′) and exon 3 (5′-GGATTTCTCCTCCCCAGAGA-3′), as well as for *GAPDH* utilized as an internal control with primers for the boundary of exons 2/3 (5′-TCGGAGTCAACGGATTTGGTCG-3′) and the boundary of exons 4/5 (5′-TTGGAGGGATCTCGCTCCTG-3′).

Results

Mutation Analysis

Mutation analysis identified two heterozygous mutations of *TACR3* in a female patient, i.e. a nonsense mutation at exon 1 (Y145X) and a single nucleotide (G) deletion from the conserved 'GT' splice donor site of intron 1 (IVS1+1delG; fig. 1A, b). The father was heterozygous for Y145X, and the mother was heterozygous for IVS1+1delG. No demonstrable mutation was detected for *TAC3* in this patient and for *TAC3* and *TACR3* in the remaining 56 cases.

Prediction of Aberrant Splicing and NMD

The IVS1+1delG mutation was predicted to add a 1,153-bp intronic sequence to exon 1 and to cause aberrant splice formation between the added sequence and the normal splice acceptor site of exon 2 (fig. 1C). Furthermore, because of the presence of a stop codon on the added intronic sequence, the IVS1+1delG mutation was predicted to cause a premature termination at the 210th codon. Thus, both IVS1+1delG and Y145X satisfied the conditions for the occurrence of NMD.

PCR-Based cDNA Screening for TACR3

TACR3 expression was clearly identified in the hypothalamus and the pituitary as well as in the whole brain, the ovary, the placenta, and the fetal kidney, but not detected in the testis and leukocytes (fig. 2).

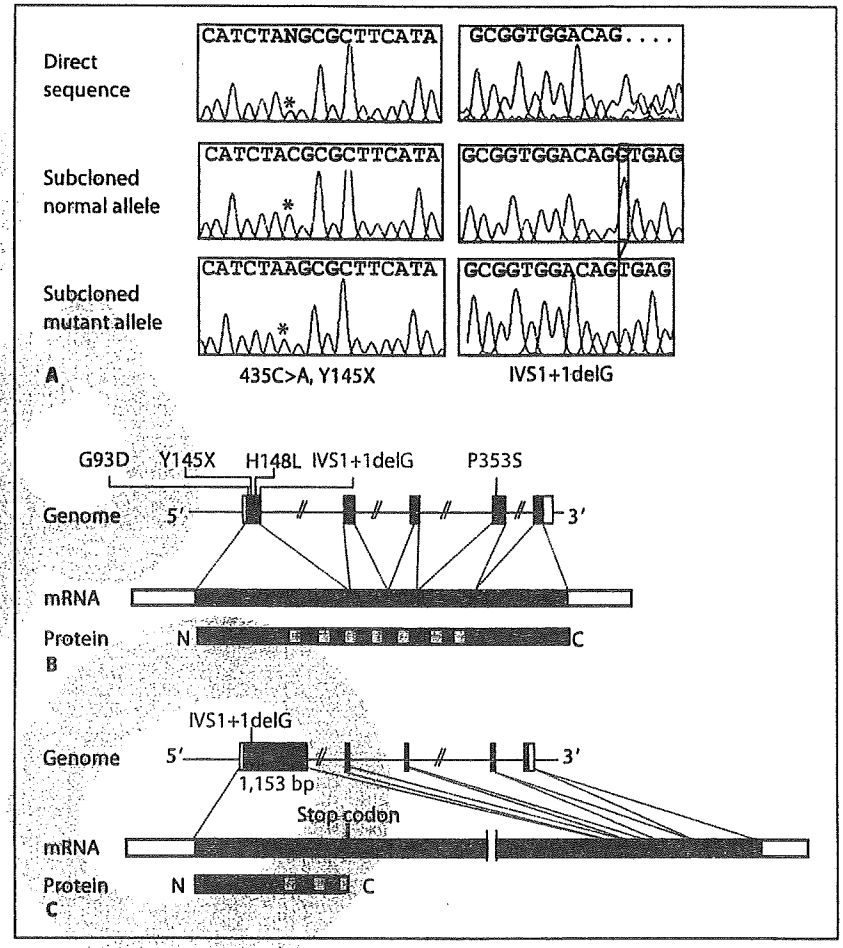

Fig. 1. *TACR3* mutations of the female Japanese patient. **A** Electrochromatograms showing 435C>A (Y145X; indicated by asterisks) and IVS1+1delG (highlighted by red lines). The mutation was indicated by direct sequencing, and confirmed by the subsequently performed sequencing of the subcloned normal and mutant alleles. **B** Schematic presentation of the positions of the mutations. The gray and white boxes on genomic DNA (Genome) and mRNA indicate the coding regions and the untranslated regions on exons 1–5. TACR3 protein (Protein) harbors 7 transmembrane domains (yellow boxes). The mutations identified in the Japanese patient are shown in red, and those reported by Topaloglu et al. [2] and Guran et al. [3] are shown in blue. **C** Predicted consequences of the IVS1+1delG mutation. In silico analysis indicates that IVS1+1delG causes addition of 1,153-bp intronic sequences (green box) to exon 1 and an aberrant splice formation between the added sequence and the normal splice acceptor site of exon 2. The transcribed intronic sequence (green box) harbors a stop codon on its very proximal 5′ region.

Case Report

This Japanese female patient was born as the sole child to nonconsanguineous parents at 42 weeks of gestation after an uncomplicated pregnancy and delivery. Her postnatal growth and development were normal until pubertal age. At 19 years of age, she was seen at a local clinic because of primary amenorrhea. She exhibited poor pubertal development (breast, Tanner stage 1; pubic hair, stage 2), with low basal gonadotropin and estradiol values (table 1). Thus, she received cyclic estrogen and progesterone therapy, and showed periodic withdrawal bleeding. She showed markedly high educational achievement at a university.

At 24 years of age, she was referred to us for further investigations. She measured 163 cm (+0.7 SD) and weighed 48.5 kg (–0.6 SD). Her breast development was at Tanner stage 3–4, and her pubic hair at stage 4. Magnetic resonance imaging delineated normal pituitary structure. Basal blood hormone values measured at 4 weeks after discontinuation of the hormone replacement therapy were consistent with IHH (table 1). Furthermore, while an initial standard GnRH test showed a poor gonadotropin response, the second-time GnRH test performed after GnRH priming (100 μg i.m. for 5 consecutive days) revealed obviously ameliorated gonadotropin responses (table 1).

The 58-year-old mother had menarche at 14.6 years of age (the menarchial age of Japanese females is 9.75–14.75 years). Subsequently, she had regular but long (~45 days) menstrual cycles with occasionally slight intermenstrual bleeding. She had no signs of androgen excess such as hirsutism. She married at 25 years of age, and failed to conceive for 3 years despite an ordinary conjugal life. Basal body temperature records indicated frequent, though not invariable, occurrence of monophasic cycles. Thus, she was treated with chlomiphene citrate by a local medical doctor, and became pregnant at the second cycle of this therapy. Polycystic ovary was excluded by repeatedly performed ultrasound studies during pregnancy. Her menses became irregular from ~45 years of age and ceased at 56 years of age (the menopausal age of Japanese females is 45–56 years). She was otherwise healthy with normal stature (150 cm, –0.5 SD for her age) and intelligence. The 59-year-old father was clinically normal with normal stature (168 cm, +0.9 SD for his age) and intelligence. Allegedly, he had an age-appropriate pubertal development and started shaving at 16 years of age.

Table 1. Endocrine data of the mutation-positive Japanese female

Hormone	Stimulus	Patient		Reference values[1]	
		basal	peak	basal	peak
Examinations at 19 years of age					
LH, mIU/ml		0.4		1.1–4.5	
FSH, mIU/ml		1.7		2.0–6.0	
Estradiol, pg/ml		<4.0		11–82	
Examinations at 24 years of age					
LH, mIU/ml	GnRH[2, 3]	<0.2	0.6	1.1–4.5	2.0–9.2
LH, mIU/ml	GnRH (after priming)[2, 4]	0.3	6.4	1.1–4.5	2.0–9.2[5]
FSH, mIU/ml	GnRH (after priming)[2, 4]	2.2	9.6	2.0–6.0	4.5–12.0[5]
Estradiol, pg/ml		15		11–82	
Prolactin, ng/ml		12.6		2.4–18.7	
TSH, mIU/l		0.75		0.30–4.50	
GH, ng/ml		8.3		<0.1–10.0	
ACTH, pg/ml		8.0		7–56	
AMH, ng/ml		3.4		0.1–7.4	

[1] Reference values in age-matched Japanese females.
[2] Hormone replacement therapy was discontinued for 4 weeks before GnRH tests.
[3] GnRH 100-μg bolus i.v. and blood sampling at 0, 30, 60, 90, and 120 min; FSH was not measured.
[4] GnRH 100-μg bolus i.v. after priming with GnRH 100 μg i.m. for 5 consecutive days.
[5] Reference peak values in a standard GnRH test; there are no reference data after GnRH priming.

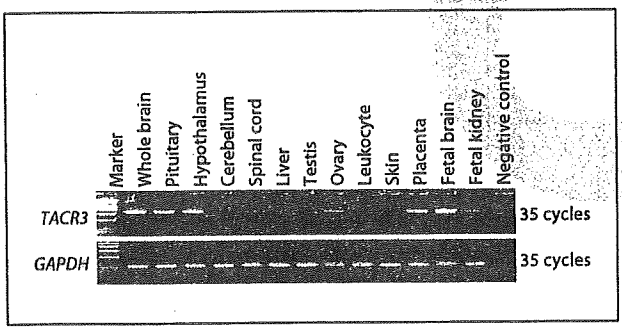

Fig. 2. PCR-based human cDNA screening for *TACR3*. *GAPDH* = Glyceraldehyde-3-phosphate dehydrogenase.

Discussion

This patient had compound heterozygous mutations of *TACR3*. In this regard, both IVS1+1delG and Y145X were predicted as a pathologic mutation missing most of the transmembrane domains. Furthermore, although mRNA was not studied because of absent *TACR3* expression in available leukocytes, both Y145X and IVS1+1delG were predicted to undergo NMD. Thus, the results provide further support for *TACR3* mutations being involved in IHH. Furthermore, the results of the 57 cases suggest the rarity of *TAC3* and *TACR3* mutations in IHH (none for *TAC3* and 1.8% for *TACR3*).

In this patient, it is notable that gonadotropin responses to GnRH stimulation were ameliorated after GnRH priming. This may suggest that the primary lesion for IHH resides in the hypothalamus rather than in the pituitary. Indeed, TACR3 protein is strongly expressed in the human hypothalamus (fig. 2) [6]. Furthermore, rodent Tacr3, Kiss1r (Gpr54), and Gnrh1 proteins are clearly expressed in the median eminence that regulates pulsatile GnRH secretion [7, 8], and human TAC3, KISS1, and ESR1 proteins are co-expressed in the infundibular nucleus that modulates estrogen feedback for gonadotropin secretion [9, 10]. In addition, hypertrophy of TAC3-positive neurons and increased *TAC3* expression have been observed in the hypothalamus of postmenopausal females with hypoestrinism [9]. These data suggest that a molecular network involving TAC3/TACR3, KISS1/KISS1R, and estrogen/ESR1 may underlie the regulation of GnRH secretion in the hypothalamus.

The heterozygous mother exhibited several clinical features suggestive of mild IHH [11]. While such manifestations are apparently absent from the previously re-

ported females heterozygous for *TACR3* missense mutations (G93D, P353S, and H148L) [2, 3], this may be due to the residual activity being retained by the missense mutations but not by the splice donor site mutation of the mother, or to the ethnic difference. Similarly, while the heterozygous father of this patient apparently lacked discernible clinical features, this may be due to sex dimorphism that GnRH secretion remains fairly constant in males and shows dynamic change with menstrual cycles in females [11, 12].

In this study, it appears worthwhile to point out that *TACR3* was clearly expressed in the ovary, but not in the testis. Although the role of *TACR3* in ovarian tissue has not been well studied, a possible involvement of *TACR3* in the development of the corpus luteum has been suggested [13]. Thus, *TACR3* mutations may also have exerted a direct impact on the ovarian function in this patient, independent of gonadotropin deficiency. In addition, the gonadal expression pattern of *TACR3* may be relevant to the phenotypic difference between the mother and father.

In summary, the present study suggests a probable hypothalamic dysfunction in patients with biallelic *TACR3* mutations and heterozygous manifestation in females, together with the rarity of *TAC3* and *TACR3* mutations in patients with IHH. Further studies will help to clarify the clinical and molecular characteristics in *TACR3* mutations.

References

1 Achermann JC, Hughes IA: Disorders of sex development; in Kronenberg HM, Melmed M, Polonsky KS, Larsen PR (eds): Williams Textbook of Endocrinology, ed 11. Philadelphia, Saunders, 2008, pp 783–848.

2 Topaloglu AK, Reimann F, Guclu M, Yalin AS, Kotan LD, Porter KM, Serin A, Mungan NO, Cook JR, Ozbek MN, Imamoglu S, Akalin NS, Yuksel B, O'Rahilly S, Semple RK: TAC3 and TACR3 mutations in familial hypogonadotropic hypogonadism reveal a key role for neurokinin B in the central control of reproduction. Nat Genet 2009;41:354–358.

3 Guran T, Tolhurst G, Bereket A, Rocha N, Porter K, Turan S, Gribble FM, Kotan LD, Akcay T, Atay Z, Canan H, Serin A, O'Rahilly S, Reimann F, Semple RK, Topaloglu AK: Hypogonadotropic hypogonadism due to a novel missense mutation in the first extracellular loop of the neurokinin B receptor. J Clin Endocrinol Metab 2009;94:3633–3639.

4 Almeida TA, Rojo J, Nieto PM, Pinto FM, Hernandez M, Martín JD, Candenas ML: Tachykinins and tachykinin receptors: structure and activity relationships. Curr Med Chem 2004;11:2045–2081.

5 Kuzmiak HA, Maquat LE: Applying nonsense-mediated mRNA decay research to the clinic: progress and challenges. Trends Mol Med 2006;12:306–316.

6 Koutcherov Y, Ashwell KW, Paxinos G: The distribution of the neurokinin B receptor in the human and rat hypothalamus. Neuroreport 2000;11:3127–3131.

7 Krajewski SJ, Anderson MJ, Iles-Shih L, Chen KJ, Urbanski HF, Rance NE: Morphologic evidence that neurokinin B modulates gonadotropin-releasing hormone secretion via neurokinin 3 receptors in the rat median eminence. J Comp Neurol 2005;489:372–386.

8 Messager S, Chatzidaki EE, Ma D, Hendrick AG, Zahn D, Dixon J, Thresher RR, Malinge I, Lomet D, Carlton MB, Colledge WH, Caraty A, Aparicio SA: Kisspeptin directly stimulates gonadotropin-releasing hormone release via G protein-coupled receptor 54. Proc Natl Acad Sci USA 2005;102:1761–1766.

9 Rance NE: Menopause and the human hypothalamus: evidence for the role of kisspeptin/neurokinin B neurons in the regulation of estrogen negative feedback. Peptides 2009;30:111–122.

10 Rometo AM, Krajewski SJ, Voytko ML, Rance NE: Hypertrophy and increased kisspeptin gene expression in the hypothalamic infundibular nucleus of postmenopausal women and ovariectomized monkeys. J Clin Endocrinol Metab 2007;92:2744–2750.

11 Bulun SE, Adashi EY: The physiology and pathology of the female reproductive axis; in Kronenberg HM, Melmed M, Polonsky KS, Larsen PR (eds): Williams Textbook of Endocrinology, ed 11. Philadelphia, Saunders, 2008, pp 541–614.

12 Goh HH, Ratnam SS: The LH surge in humans: its mechanism and sex difference. Gynecol Endocrinol 1988;2:165–182.

13 Brylla E, Aust G, Geyer M, Uckermann O, Löffler S, Spanel-Borowski K: Coexpression of preprotachykinin A and B transcripts in the bovine corpus luteum and evidence for functional neurokinin receptor activity in luteal endothelial cells and ovarian macrophages. Regul Pept 2005;125:125–133.

Heterozygous Orthodenticle Homeobox 2 Mutations Are Associated with Variable Pituitary Phenotype

Sumito Dateki, Kitaro Kosaka, Kosei Hasegawa, Hiroyuki Tanaka, Noriyuki Azuma, Susumu Yokoya, Koji Muroya, Masanori Adachi, Toshihiro Tajima, Katsuaki Motomura, Eiichi Kinoshita, Hiroyuki Moriuchi, Naoko Sato, Maki Fukami, and Tsutomu Ogata

Department of Endocrinology and Metabolism (S.D., N.S., M.F., T.O.), National Research Institute for Child Health and Development, and Division of Ophthalmology (N.A.) and Department of Medical Subspecialties (S.Y.), National Children's Medical Center, Tokyo 157-8535, Japan; Department of Pediatrics (S.D., K.M., E.K., H.M.), Nagasaki University Graduate School of Biomedical Sciences, Nagasaki 852-8501, Japan; Department of Pediatrics (K.K.), Kyoto Prefectural University of Medicine, Graduate School of Medical Science, Kyoto 602-8566, Japan; Department of Pediatrics (K.H., H.T.), Okayama University Graduate School of Medicine, Dentistry, and Pharmaceutical Sciences, Okayama 700-8558, Japan; Division of Endocrinology and Metabolism (K.M., M.A.), Kanagawa Children's Medical Center, Yokohama 232-8555, Japan; and Department of Pediatrics (T.T.), Hokkaido University School of Medicine, Sapporo 060-8638, Japan

Context: Although recent studies have suggested a positive role of *OTX2* in pituitary as well as ocular development and function, detailed pituitary phenotypes in *OTX2* mutations and *OTX2* target genes for pituitary function other than *HESX1* and *POU1F1* remain to be determined.

Objective: We aimed to examine such unresolved issues.

Subjects: We studied 94 Japanese patients with various ocular or pituitary abnormalities.

Results: We identified heterozygous p.K74fsX103 in case 1, p.A72fsX86 in case 2, p.G188X in two unrelated cases (3 and 4), and a 2,860,561-bp microdeletion involving *OTX2* in case 5. Clinical studies revealed isolated GH deficiency in cases 1 and 5; combined pituitary hormone deficiency in case 3; abnormal pituitary structures in cases 1, 3, and 5; and apparently normal pituitary function in cases 2 and 4, together with ocular anomalies in cases 1–5. The wild-type Orthodenticle homeobox 2 (OTX2) protein transactivated the *GNRH1* promoter as well as the *HESX1*, *POU1F1*, and *IRBP* (interstitial retinoid-binding protein) promoters, whereas the p.K74fsX103-OTX2 and p.A72fsX86-OTX2 proteins had no transactivation functions and the p.G188X-OTX2 protein had reduced (~50%) transactivation functions for the four promoters, with no dominant-negative effect. cDNA screening identified positive *OTX2* expression in the hypothalamus.

Conclusions: The results imply that *OTX2* mutations are associated with variable pituitary phenotype, with no genotype-phenotype correlations, and that *OTX2* can transactivate *GNRH1* as well as *HESX1* and *POU1F1*. (***J Clin Endocrinol Metab* 95: 756–764, 2010**)

Pituitary development and function depends on the spatially and temporally controlled expression of multiple transcription factor genes such as *POU1F1*, *HESX1*, *LHX3*, *LHX4*, *PROP1*, and *SOX3* (1, 2). Whereas mutations of some genes (*e.g. POU1F1*) result in a relatively characteristic pattern of pituitary hormone deficiency, those of other genes (*e.g. HESX1*) are associated with a wide range of pituitary phenotype including combined pi-

ISSN Print 0021-972X ISSN Online 1945-7197
Printed in U.S.A.

doi: 10.1210/jc.2009-1334 Received June 23, 2009. Accepted November 9, 2009.
First Published Online December 4, 2009

Abbreviations: CGH, Comparative genomic hybridization; CPHD, combined pituitary hormone deficiency; EPP, ectopic posterior pituitary; FISH, fluorescence *in situ* hybridization; HD, homeodomain; IGHD, isolated GH deficiency; IRBP, interstitial retinoid-binding protein; MLPA, multiplex ligation-dependent probe amplification; NMD, nonsense mediated mRNA decay; OTX2, orthodenticle homeobox 2; PH, pituitary hypoplasia; SOD, septooptic dysplasia; TD, transactivation domain.

tuitary hormone deficiency (CPHD), isolated GH deficiency (IGHD), and apparently normal phenotype. However, because mutations of these genes account for a relatively minor portion of patients with congenital hypopituitarism (2, 3), multiple genes would remain to be identified in congenital hypopituitarism.

Orthodenticle homeobox 2 (*OTX2*) is a transcription factor gene primarily involved in ocular development (4). It encodes a paired type homeodomain (HD) and a transactivation domain (TD) and produces two functionally similar splice variants, isoform-a (GenBank accession no. NM_21728.2) and isoform-b (NM_172337.1) with and without eight amino acids because of alternative splice acceptor sites at the boundary of intron 3 and exon 4 (5). To date, at least 10 pathological heterozygous *OTX2* mutations have been identified in patients with ocular malformations such as anophthalmia and/or microphthalmia (6, 7). Ocular phenotype is highly variable, ranging from anophthalmia to nearly normal eye development, even in patients from the same family. Furthermore, most patients also exhibit brain anomaly, seizure, and/or developmental delay.

Recent studies have indicated that *OTX2* is also involved in pituitary development and function. Dateki *et al.* (8) showed that *OTX2* is expressed in the pituitary and has a transactivation function for the promoters of *POU1F1* and *HESX1* as well as the promoter of *IRBP* (interstitial retinoid-binding protein) involved in ocular function and that a frameshift *OTX2* mutation identified in a patient with bilateral anophthalmia and partial IGHD barely retained the transactivation activities. Subsequently a missense *OTX2* mutation with a dominant-negative effect and a frameshift *OTX2* mutation with loss-of-function effect were identified in CPHD patients with and without ocular malformation (9, 10).

However, detailed pituitary phenotypes in *OTX2* mutation-positive patients as well as other possible *OTX2* target genes for pituitary development and function remain to be determined. Here we report five new patients with *OTX2* mutations and summarize clinical findings in *OTX2* mutation-positive patients. We also show that *OTX2* is expressed in the hypothalamus and has a transactivation function for the promoter of *GNRH1*.

Patients and Methods

Patients

We studied 94 Japanese patients consisting of: 1) 16 patients with ocular anomalies and pituitary dysfunctions accompanied by short stature (<−2 SD) (six with anophthalmia and/or microphthalmia and CPHD, five with anophthalmia and/or microphthalmia and IGHD, three with septooptic dysplasia (SOD) and CPHD, and two with SOD and IGHD) (group 1); 2) 12 patients with ocular anomalies whose pituitary functions were not investigated (one with bilateral microphthalmia and short stature, one with bilateral optic nerve hypoplasia and short stature, and 10 with anophthalmia and/or microphthalmia and normal stature) (group 2); and 3) 66 patients with pituitary dysfunctions but without ocular anomalies (five with IGHD and 61 patients with CPHD) (group 3). No demonstrable mutation was identified for *HESX1* in patients with SOD, *GH1* and *HESX1* in patients with IGHD, and *POU1F*, *HESX1*, *LHX3*, *LHX4*, *PROP1*, and *SOX3* in patients with various types of CPHD (2). All the patients had normal karyotype.

Primers and probes

The primers and probes used in this study are shown in Supplemental Table 1, published as supplemental data on The Endocrine Society's Journals Online web site at http://jcem.endojournals.org.

Sequence analysis of OTX2

This study was approved by the Institutional Review Board Committee at National Center for Child Health and Development. After obtaining written informed consent, the coding exons 3-5 and their flanking splice sites were PCR amplified using leukocyte genomic DNA samples of all 94 patients and were subjected to direct sequencing on a CEQ 8000 autosequencer (Beckman Coulter, Fullerton, CA). To confirm a heterozygous mutation, the corresponding PCR products were subcloned with TOPO TA cloning kit (Invitrogen, Carlsbad, CA), and normal and mutant alleles were sequenced separately.

Prediction of the occurrence of aberrant splicing and nonsense mediated mRNA decay (NMD)

To examine whether identified mutations could cause aberrant splicing by creating or disrupting exonic splicing enhancers and/or splice sites (11, 12), we performed *in silico* analyses with the ESE finder release 3.0 (http://rulai.cshl.edu/cgi-bin/tools/ESE3/esefinder.cgi) for the prediction of exonic splice enhancers and with the program at the Berkeley Drosophila Genome Project (http://www.fruitfly.org/seq_tools/splice.html) for the prediction of splice sites. We also analyzed whether identified mutations could be subject to NMD on the basis of the previous report (12, 13).

Deletion analysis

Multiplex ligation-dependent probe amplification (MLPA) was performed for *OTX2* intragenic mutation-negative patients as a screening of a possible microdeletion affecting *OTX2*. This procedure was performed according to the manufacturer's instructions (14), using probes designed specifically for *OTX2* exon 4 together with a commercially available MLPA probe mix (P236) (MRC-Holland, Amsterdam, The Netherlands) used as internal controls. To confirm a microdeletion, fluorescence *in situ* hybridization (FISH) was performed with a long PCR product for *OTX2* (a 6096 bp segment from intron 2 to exon 5) together with an RP11-566I2 BAC probe (14q11.2; Invitrogen, Carlsbad, CA) used as an internal control. The probe for *OTX2* was labeled with digoxigenin and detected by rhodamine anti-digoxigenin, and the control probe was labeled with biotin and

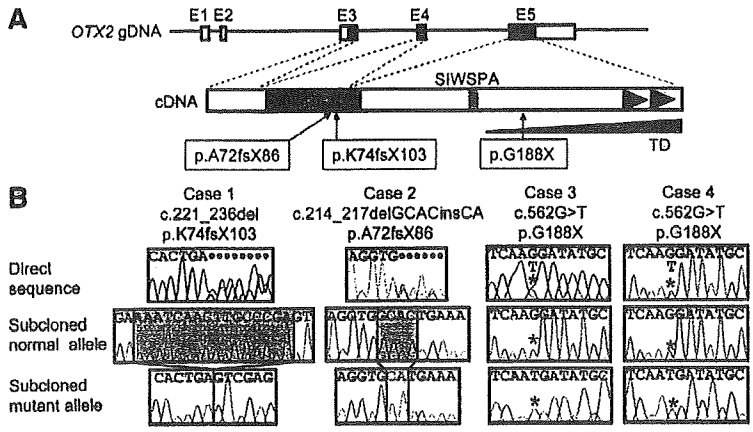

FIG. 1. Sequence analysis in cases 1–4. A, The structure of *OTX2* (the isoform-b) and the position of the mutations identified. The *black* and *white boxes* on genomic DNA (gDNA) denote the coding regions on exons 1-5 (E1-E5) and the untranslated regions, respectively. *OTX2* encodes the HD (a *blue region*), the SIWSPA conserved motif (an *orange region*), and the two tandem tail motifs (*green triangles*). The TD (a *gray triangle*) is assigned to the C-terminal side; deletion of each tail motif reduces the transactivation function, and that of a region distal to the SIWSPA motif further reduces the transactivation function. In addition, another TD may also reside in the 5′ side of the HD (17). The three mutations identified in this study are shown. B, Electrochromatograms showing the mutations in cases 1–4. Shown are the direct sequences and subcloned normal and mutant sequences. The deleted sequences are shaded in *gray*, and the inserted sequence is highlighted in *yellow*. The mutant and the corresponding wild-type nucleotides are indicated by *red asterisks*.

detected by avidin conjugated to fluorescein isothiocyanate. To indicate an extent of a microdeletion, oligoarray comparative genomic hybridization (CGH) was carried out with 1×244K human genome array (catalog no. G4411B; Agilent Technologies, Palo Alto, CA), according to the manufacturer's protocol. Finally, to characterize a microdeletion, long PCR was performed with primer pairs flanking the deleted region, and a long PCR product was subjected to direct sequencing using serial sequence primers. The deletion size and the junction structure were determined by comparing the obtained sequences with the reference sequences at the National Center for Biotechnology Information Database (NC_000014.7; Bethesda, MD), and the presence or absence of repeat sequences around the breakpoints was examined with Repeatmasker (http://www.repeatmasker.org).

Functional studies

Western blot analysis, subcellular localization analysis, DNA binding analysis, and transactivation analysis were performed by the previously reported methods (8) (for details, see Supplemental Methods). In this study, we used the previously reported expression vector and fluorescent vector containing the wild-type *OTX2* cDNA; the probes with the wild-type and mutated OTX2 binding sites within the *IRBP*, *HESX1*, and *POU1F1* promoter sequences; and the luciferase reporter vectors containing the *IRBP*, *HESX1*, and *POU1F1* promoter sequences (8). We further created expression vectors and fluorescent vectors containing mutant *OTX2* cDNAs by site-directed mutagenesis using Prime STAR mutagenesis basal kit (Takara, Otsu, Japan), and constructed a 30-bp probe with wild-type (TAATCT) and mutated (TGGGCT) putative OTX2 binding site within the *GNRH1* promoter sequence and a luciferase reporter vector containing the *GNRH1* promoter sequence (−1349 to −1132 bp) by inserting the corresponding sequence into pGL3 basic. The *GNRH1* promoter sequence was based on the report of Kelley *et al.* (15). Transfections were performed in triplicate within a single experiment, and the experiment was repeated three times.

PCR-based expression analysis of *OTX2*

Human cDNA samples were purchased from CLONTECH (Palo, Alto, CA) except for leukocyte and skin fibroblast cDNA samples that were prepared with Superscript III reverse transcriptase (Invitrogen). PCR amplification was performed for the cDNA samples (0.5 ng), using the primers hybridizing to exon 3 and 4 of *OTX2* and those hybridizing to exons 2/3 and 4/5 (boundaries) of *GAPDH* used as an internal control.

Results

Identification of mutations and substitutions

Three novel heterozygous *OTX2* mutations were identified in four cases, *i.e.* a 16-bp deletion at exon 4 that is predicted to cause a frameshift at the 74th codon for lysine and resultant termination at the 103rd codon (c.221_236del16, p.K74fsX103) in case 1; a 4-bp deletion and a 2-bp insertion at exon 4 that is predicted to cause a frame shift at the 72nd codon for alanine and resultant termination at the 86th codon (c.214_217delGCACinsCA, p.A72fsX86) in case 2; and a nonsense mutation at exon 5 that is predicted to cause a substitution of the 188th glycine with stop codon (c.562G>T, p.G188X) in two unrelated cases (3 and 4; Fig. 1). In addition, heterozygous missense substitutions were identified in patient 1 (c.532A>T, p.T178S) and patient 2 (c.734C>T, p.A245V). Cases 1 and 3 were from group 1, cases 2 and 4 and patient 2 were from group 2, and patient 1 was from group 3. Parental analysis indicated that frameshift mutations in cases 1 and 2 were absent from the parents (*de novo* mutations), whereas the missense substitution of patient 2 was inherited from phenotypically normal father. The parents of cases 3 and 4 and patient 1 refused molecular studies. All the mutations and the missense substitutions were absent from 100 control subjects.

Prediction of the occurrence of aberrant splicing and NMD

The two frameshift mutations and the nonsense mutation were predicted to influence neither exonic splice enhancers nor splice donor and acceptor sites (Supplemental Tables 2 and 3). Furthermore, the two frameshift mutations were predicted to produce the premature termination codons on the mRNA transcribed from the last exon

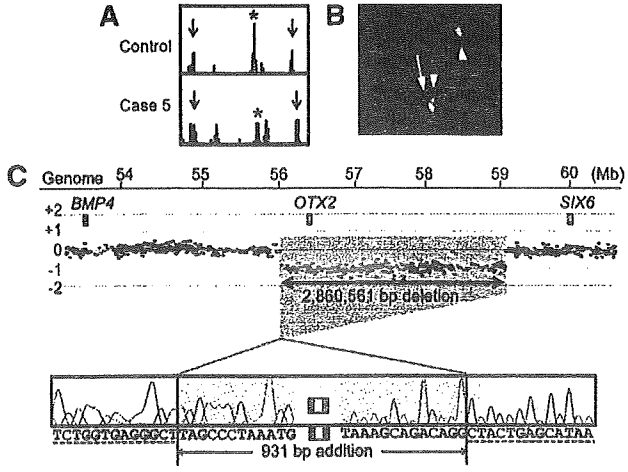

FIG. 2. Deletion analysis in case 5. A, MLPA analysis. The *red asterisk* indicates peaks for the *OTX2* exon 4, and the *black arrows* indicate control peaks. The *red peaks* indicate the internal size markers. Deletion of the MLPA probe binding site is indicated by the reduced peak height. B, FISH analysis. The probe for *OTX2* detects only a *single red signal* (an *arrow*), whereas the RP11-566I2 BAC probe identifies *two green signals* (*arrowheads*). C, Oligoarray CGH analysis and direct sequencing of the deletion junction. The deletion is 2,860,561 bp in physical size (shaded in *gray*) and is associated with an addition of a 931-bp segment (highlighted in *yellow*). The normal sequences flanking the microdeletion are indicated with *dashed underlines*.

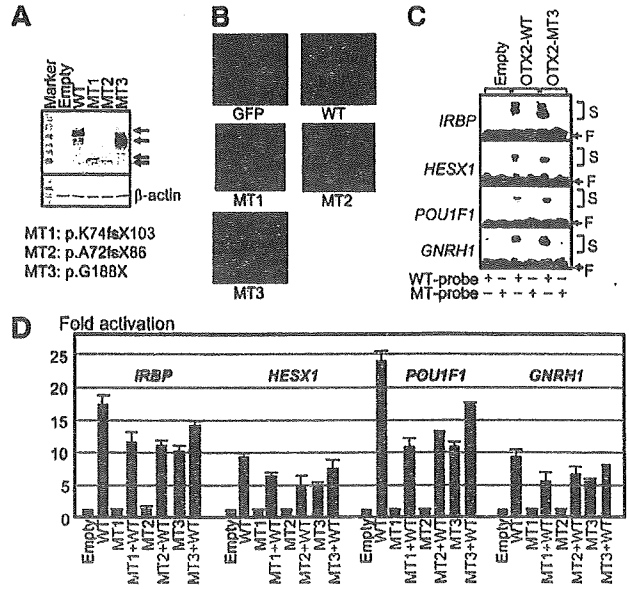

FIG. 3. Functional studies. A, Western blot analysis. Both WT and MT1-MT3 OTX2 proteins are detected with different molecular masses (*arrows*). WT, Wild type; MT1, p.K74fsX103; MT2, p.A72fsX86; and MT3, p.G188X. B, Subcellular localization analysis. Whereas green fluorescent protein (GFP) alone is diffusely distributed throughout the cell, the GFP-fused WT-OTX2 and MT3-OTX2 proteins localize to the nucleus. By contrast, the GFP-fused MT1-OTX2 and MT2-OTX2 proteins are incapable of localizing to the nucleus. C, DNA binding analysis using the wild-type (WT) and mutated (MT) probes derived from the promoters of *IRBP*, *HESX1*, *POU1F1*, and *GNRH1*. The symbols (+) and (–) indicate the presence and absence of the corresponding probes, respectively. Both WT and MT3 OTX2 proteins bind to the WT but not the MT probes. For the probe derived from the *IRBP* promoter, two shifted bands are found for both WT-OTX2 and MT3-OTX2 proteins as reported previously (17). S, Shifted bands; F, free probes. D, Transactivation analysis, using the promoter sequences of *IPBP*, *HESX1*, *POU1F1*, and *GNRH1*. The results are expressed using the mean and SD. The *black*, *blue*, *red*, and *green bars* indicate the data of the empty expression vectors (0.6 μg), expression vectors with WT *OTX2* cDNA (0.6 μg), expression vectors with MT1-MT3 *OTX2* cDNAs (0.6 μg), and the mixture of expression vectors with WT (0.3 μg) and those with MT1-MT3 *OTX2* cDNAs (0.3 μg), respectively; thus, the same amount of expression vectors has been used for each assay.

5, indicating that the frameshift mutations as well as the nonsense mutation had the property to escape NMD (Supplemental Fig. 1).

Identification of a microdeletion

A heterozygous microdeletion affecting *OTX2* was indicated by MLPA and confirmed by FISH in case 5 of group 1 (Fig. 2, A and B). Oligoarray CGH delineated an approximately 2.9-Mb deletion, and sequencing of the fusion point showed that the microdeletion was 2,860,561 bp in physical size (56,006,531–58,867,091 bp on the NC_000014.7) and was associated with an addition of a complex 931-bp segment consisting of the following structures (cen → tel): 2 bp (TA) insertion → 895 bp sequence identical with that in a region just centromeric to the microdeletion (55, 911, 347–55, 912, 241 bp) → 1 bp (C) insertion → 33-bp sequence identical with that within the deleted region (58, 749, 744–58, 749, 776 bp) (Fig. 2C). Repeat sequences were absent around the break points. This microdeletion was not detected in DNA from the parents.

Functional studies of the wild-type and mutant OTX2 proteins

Western blot analysis detected wild-type OTX2 protein of 31.6 kDa and mutant OTX2 proteins of 11.5 kDa (p.K74fsX103), 9.7 kDa (p.A72fsX86), and 15.4 kDa (p.G188X) (Fig. 3A). The molecular masses were as predicted from the mutations. The band intensity was comparable between the wild-type OTX2 protein and the p.G188X-OTX2 protein and was faint for the p.K74fsX103-OTX2 and p.A72fsX86-OTX2 proteins.

Subcellular localization analysis showed that the p.G188X-OTX2 protein localized to the nucleus as did the wild-type OTX2 protein, whereas the p.K74fsX103-OTX2 and p.A72fsX86-OTX2 proteins were incapable of localizing to the nucleus (Fig. 3B). The results were consistent with those of the Western blot analysis because nuclear extracts were used for the Western blotting, with some probable contamination of cytoplasm.

DNA binding analysis revealed that the p.G188X-OTX2 protein with nuclear localizing capacity bound to the wild-type OTX2 binding sites within the four promoters examined, including the *GNRH1* promoter, but not to the mutated OTX2 binding sites (Fig. 3C). The band shift

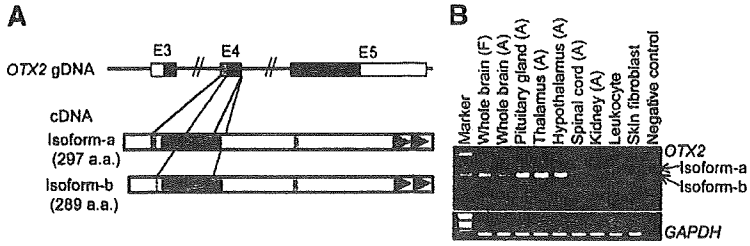

FIG. 4. PCR-based human cDNA library screening for *OTX2* (35 cycles). A, Schematic representation of the *OTX2* isoform-a (NM_21728.2) and isoform-b (NM_172337.1). Because of the two alternative splice acceptor sites at the boundary between intron 3 and exon 4, isoform-a carries eight amino acids (shown in *gray*) in the vicinity of the HD, whereas isoform-b is lacking the eight amino acids. B, PCR amplification data. *OTX2* is clearly expressed in the pituitary and hypothalamus, with isoform-b being the major product. *GAPDH* has been used as an internal control. F, Fetus; A, adult.

was more obvious for the wild-type OTX2 protein than for the p.G188X-OTX2 protein, consistent with the difference in the molecular masses.

Transactivation analysis showed that the wild-type OTX2 protein had transactivation activities for the four promoters examined including the *GNRH1* promoter, whereas the p.K74fsX103-OTX2 and p.A72fsX86-OTX2 proteins had virtually no transactivation function, and the p.G188X-OTX2 protein had reduced (~50%) transactivation activities (Fig. 3D). The three mutant OTX2 proteins had no dominant-negative effects. In addition, the two missense p.A245V-OTX2 and p.T178S-OTX2 proteins had apparently normal transactivation activities with no dominant-negative effect (Supplemental Fig. 2).

PCR-based expression analysis of *OTX2*

OTX2 expression was identified in the pituitary and the hypothalamus as well as in the brain and the thalamus but not detected in the spinal cord, kidney, leukocytes, and skin fibroblasts (Fig. 4). The isoform-b lacking the eight amino acids was predominantly expressed.

Clinical findings in *OTX2* mutation-positive patients

Clinical data are summarized in Table 1 (*left part*). Anophthalmia and/or microphthalmia was present in cases 1–5. Developmental delay was obvious in cases 1 and 3–5, whereas it was obscure in case 2 because of the young age. Prenatal growth was normally preserved in cases 1–5, whereas postnatal growth was compromised in cases 1, 3, and 5. Cases 1 and 5 had IGHD, and case 3 had CPHD (Table 2); furthermore, cases 1, 3, and 5 had pituitary hypoplasia (PH) and/or ectopic posterior pituitary (EPP) (Supplemental Fig. 3). Case 3 showed no pubertal development at 15 yr of age (Tanner pubic hair stage 2 in Japanese boys: 12.5 ± 0.9 yr) (16). Cases 2 and 4 had no discernible pituitary dysfunction and did not receive magnetic resonance imaging examinations. In addition, case 1 had right retractile testis. Patient 1 with p.T178S had CPHD but without ocular anomalies, and patient 2 with p.A245V had bilateral optic nerve hypoplasia and short stature.

Discussion

We identified two frameshift mutations in cases 1 and 2 and a nonsense mutation in unrelated cases 3 and 4. Furthermore, it was predicted that these mutations neither affected splice patterns nor underwent NMD, although direct analysis using mRNA was impossible due to lack of detectable *OTX2* expression in already collected leukocytes as well as skin fibroblasts, which might be available from cases 1–4. Thus, these mutations are predicted to produce aberrant OTX2 proteins *in vivo* that were used in the *in vitro* functional studies. In this context, the functional studies indicated that the two frameshift mutations were amorphic and the nonsense mutation was hypomorphic. The results are consistent with the previous notion that the HD not only has DNA binding capacity but also retains at least a part of nuclear localization signal on its C-terminal portion and the TD primarily resides in the C-terminal region (17) (Fig. 1A). Whereas the two missense substitutions were absent in 100 control subjects, they would be rare normal variations rather than pathological mutations because of the normal transactivation activities with no dominant-negative effect.

We also detected a heterozygous microdeletion involving *OTX2* in case 5 that was not mediated by repeat sequences. This implies the importance of the examination of a microdeletion. Indeed, such a cryptic microdeletion has been identified in multiple genes with the development of MLPA that can serve as a screening method in the detection of microdeletions (18). Whereas the microdeletion of case 5 has removed 16 additional genes (Ensembl Genome Browser, http://www.ensembl.org/), the clinical phenotype of case 5 is explainable by *OTX2* haploinsufficiency alone. Thus, hemizygosity for the 16 genes would not have a major clinical effect, if any.

Furthermore, the present study revealed two findings. First, *OTX2* was expressed in the hypothalamus and had a transactivation function for the *GNRH1* promoter. This implies that *GNRH1* essential for the hypothalamic GnRH secretion is also a target gene of *OTX2*, as has been demonstrated in the mouse (15). Second, the short isoform-b was predominantly identified in the *OTX2* expression-positive tissues. This sug-